Welding in the World (2023) 67:183–194
https://doi.org/10.1007/s40194-022-01410-5

RESEARCH PAPER

Hydrogen effect on mechanical properties and cracking of creep-resistant 9% Cr P92 steel and P91 weld metal

Michael Rhode[1,2] · Jonathan Nietzke[1] · Tim Richter[1] · Tobias Mente[1] · Peter Mayr[3] · Alexander Nitsche[4]

Received: 9 August 2022 / Accepted: 7 November 2022 / Published online: 19 November 2022

Abstract
Martensitic 9% Cr steels like P91 and P92 can show an increased susceptibility to delayed hydrogen-assisted cracking. The focus of this study was the microstructure and heat treatment effect on the mechanical properties of P92 base material and P91 multi-layer weld metal in both as-welded and post weld heat treated (PWHT) condition. Tensile tests with hydrogen-free reference samples and electrochemically hydrogen charged samples were carried out; the mechanical properties were assessed and supported by detailed fractographic analysis. Finally, a hydrogen and microstructure-dependent fracture criterion is established. All investigated microstructures showed a hydrogen-influenced degradation of the mechanical properties compared to the hydrogen-free reference samples. The as-welded martensitic P91 weld metal had the highest degree of degradation in the presence of hydrogen. The P91 PWHT weld metal and the P92 base material had comparable properties. From that point of view, a significantly increased risk for hydrogen-assisted cold cracking during welding fabrication of P91 weld joints must be considered before any heat treatment is conducted.

Keywords Creep-resisting materials · Diffusion · Hydrogen embrittlement · Weld metal

1 Introduction

Martensitic 9% Cr steels like P91 (X10CrMoVNb9-1) or P92 (X10CrWMoVNb9-2) represent materials with excellent creep resistance. Currently, they are widely used in thermal power plants [1, 2]. With focus on CO_2-neutral energy systems, these steel grades are also candidate structural materials for latent heat storage systems [3] and fusion reactor applications [4]. The martensitic microstructure demands careful welding fabrication of these 9% Cr steels [2]. After welding, a multi-step heat procedure must be conducted. (1) The welded components must be cooled down to approximately 80 °C to ensure a fully martensitic transformation of the welded joint. (2) Subsequently, a hydrogen removal heat treatment (HRHT) is carried out (sometimes also referred as "soaking" or dehydrogenation heat treatment/DHT), followed by cooling down to ambient/room temperature. This step is essential for the avoidance of possible delayed hydrogen-assisted cracking (HAC). Finally, (3) the welded joint is subjected to the post weld heat treatment (PWHT) at temperatures ≥ 700 °C [2, 5, 6]. The PWHT is mandatory for such steel grades in terms of both the reduction of the welding residual stresses and further desired metallurgical effects (partial dissolution of carbides, tempering of martensite, etc.) that restore the necessary mechanical properties (toughness, i.e., higher fracture resistance). If the previous mentioned second step of the HRHT is not or insufficiently applied (e.g., in terms of short dwell time), the delayed HAC is a considerable risk in welded Cr(-Mo)-based steel weld joints [7–9]. The underlying cracking mechanism is influenced by the interaction of three local factors, (1) the absorbed diffusible hydrogen concentration

Recommended for publication by Commission IX - Behaviour of Metals Subjected to Welding.

✉ Michael Rhode
michael.rhode@bam.de

[1] Bundesanstalt für Materialforschung und -prüfung (BAM), Department 9 - Component Safety, Unter den Eichen 87, Berlin, Deutschland

[2] Institute for Materials Science and Joining Technology, Otto-Von-Guericke-University, Magdeburg, Germany

[3] Department of Mechanical Engineering, Chair of Materials Engineering of Additive Manufacturing, Technical University of Munich, Garching, Germany

[4] ZABAG Security Engineering GmbH, Grünhainichen, Germany

(HD) during welding, coupled with a (2) mechanical load within a (3) susceptible microstructure [10, 11]. Martensitic 9% Cr steels generally show an increased susceptibility for HAC due to their martensitic microstructure, i.e., the limited ductility/toughness, especially in the as-welded (AW) condition [9, 12–14].

Cold cracking tests on P91 weld joints show a significant susceptibility for HAC, whereas the deposited weld metal (WM) has a higher risk then the heat-affected zone (HAZ) [15]. In addition, 9% Cr steels generally show an increased risk for HAC (e.g., compared to low-alloyed Cr–Mo steels) [9]. Typically, cold cracking tests do not allow to identify a critical (diffusible) hydrogen concentration for HAC directly. Either the test sample prepared for any cracking susceptibility test is not suitable for the detection of the hydrogen concentration [9, 15] or the test sample is optimized for hydrogen measurement (like the ISO 3690 standard [16]). A practical result is that a tolerable hydrogen concentration, where HAC does not occur for a given steel, cannot typically be estimated from such tests. In addition, the microstructure specific diffusion behavior of hydrogen in the base material (BM), HAZ and WM is not anticipated [9, 15] and corresponding literature is rare so far. For that reason, the authors published within this series of publications two studies on the diffusion behavior in P92 and P91 steel weld joints [17, 18]. The knowledge of microstructure specific data on hydrogen-influenced degradation of the material properties is very important. The focus of this study is the combined microstructure and heat treatment effect on the HAC susceptibility of P92 base material and P91 multi-layer weld metal. For that purpose, tensile tests with electrochemically hydrogen charged samples were carried out, including a detailed fractographic analysis. Finally, a hydrogen and microstructure-dependent fracture criterion is established.

2 Materials and methods

2.1 Investigated materials, welding procedure, and sample geometry

The 9% Cr steel P92/X10CrWMoVNb9-2 was investigated in terms of a tube section (VMT, former Vallourec & Mannesmann Tubes) with an inner diameter of 88.9 mm and a wall thickness of 17.5 mm. The length was 150 mm; see Fig. 1a. In the following, it is labelled as base material (BM). The BM was in normalized (1060 °C, 0.33 h, followed by air cooling) and tempered (780 °C, 1 h, air cooling) condition. As weld metal (WM), the creep-resistant martensitic 9% Cr P91/X0CrMoVNb9-1 was investigated. Manual multi-pass MAG welding was carried out, using a rutile-basic flux-cored wire (C 9 MV Ti-FD [19]). The WM was deposited on a S355 substrate plate with 15 mm thickness. The wire feed speed was 13 m/min, welding current 250 A to 270 A, welding arc voltage 25 V to 27 V, and welding speed approximately 30 cm/min to 40 cm/min. The shielding gas was a mixture of 82% Ar and 18% CO_2, the preheat temperature was 200 °C, and the interpass temperature was 280 °C, in accordance with [17, 18]. As schematically shown in Fig. 1c, this resulted in an all-weld metal block with 40 mm thickness, 60 mm width, and 160 mm length. Subsequently, the block was cut into two pieces. One part remained in the as-welded (AW) condition and the other was subjected to PWHT at 760 °C for 4 h [19, 21]).

Tensile specimens (see Sect. 2.3 for test parameters) were machined (by turning) from the respective materials and extracted at the positions described in Fig. 1a (P92 BM) and Fig. 1b (P91 WM for both the AW and PWHT condition). For avoidance of dilution effects of substrate and the deposited P91 WM, the samples had been extracted with a distance of minimum 5 mm to the substrate/WM interface. Figure 1c shows the used round tensile specimen geometry.

2.2 Chemical composition and microstructure

Table 1 shows the chemical composition of the investigated materials, which was determined by optical emission spectroscopy (OES by Spectrotest, Spectro GmbH, Germany). The measured nitrogen and boron content was close to the detection limit of the used OES equipment and includes an uncertainty. The nominal composition of the P92 BM is listed in [20] and P91 WM in [21], respectively.

The P92 BM showed a tempered martensitic microstructure (see Fig. 2a). The etching was carried out with Kalling's solution (martensitic stainless-steel etchant). The measured average hardness was 228 HV0.5 ± 5 HV0.5. The P91 AW-WM (Fig. 2b) is represented by a mostly martensite microstructure (needle-shape laths) with portions of δ-Ferrite (revealed by Lichtenegger-Bloech (LBII) etchant). The hardness was 404 HV0.5 ± 27 HV0.5. The P91 PWHT-WM microstructure (Fig. 2c) changed to a tempered martensite after the post weld heat treatment, e.g., described by the significantly reduced hardness with 271 HV0.5 ± 7 HV0.5. The P91 WM microstructure was investigated the center region of the deposited multi-layer welds in a distance of approx. 20 mm to the interface with the S355 substrate plate. This ensured a repeatable heat treatment condition in both cases the AW and the PWHT. As demonstrated in the reference [22], the microstructure is associated with precipitated M-carbonitrides (where "M" means metal, e.g., Cr, Mo, and especially V) or $M_{23}C_6$-carbides at the grain boundaries accompanied by coarsening martensite laths during the PWHT.

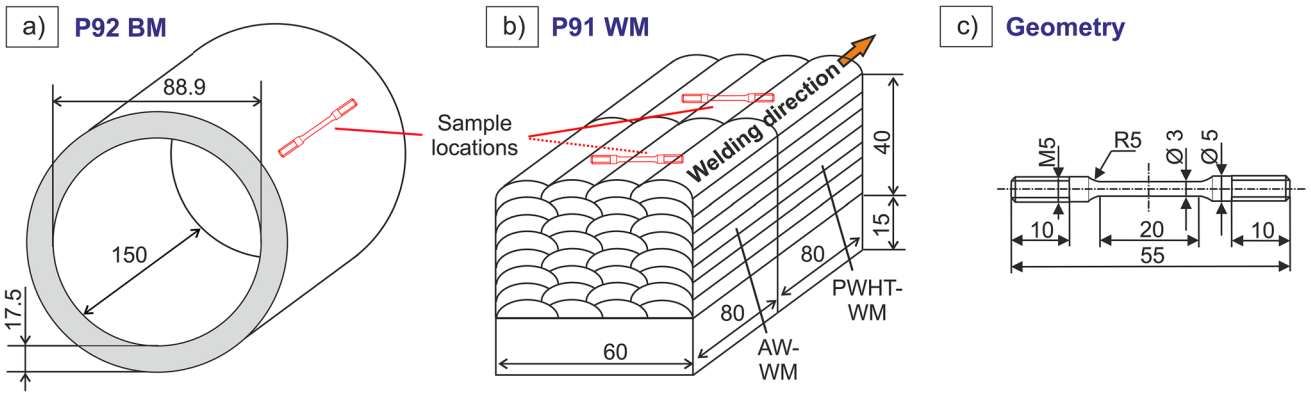

Fig. 1 Sample materials and specimen location: (a) P92 BM tube section, (b) P91 WM block, and (c) tensile specimen geometry

Table 1 Composition of P92 BM and P91 WM (in wt.—%, Fe—balance)

Grade	C	Cr	Mo	V	Si	Nb	Mn	Ni	W	N	B	P	S
P92 BM/OES	0.12	8.90	0.35	0.20	0.24	0.04	0.50	0.12	2.01	0.05	0.002	0.007	0.005
P91 WM/OES	0.09	9.50	0.96	0.20	0.21	0.03	0.80	1.40	–	0.04	–	0.009	0.007

2.3 Hydrogen charging, measurement, and tensile test

The tensile tests were performed to identify the hydrogen-dependent tensile and ductility parameters by comparison of hydrogen-free and charged tensile samples.

2.3.1 Hydrogen charging

The hydrogen charging was performed using the common cathodic charging in galvanostatic mode, i.e., constant current density, delivered by a Galvanostat Wenking TG 97 (Bank Electronics, Germany). The used electrolyte was an aqueous solution of 0.1 M H_2SO_4 (sulfuric acid) with the addition of 12 mg/l NaAsO2 (sodium arsenate) as recombination poison to prevent hydrogen recombination. The sample was the (cathodic) working electrode and the (anodic) counterpart was a Pt1800 electrode (SI Analytics, Germany). Further experimental details on the underlying absorption mechanisms can be found in [12, 23]. Before charging, each specimen was cleaned in acetone using an ultrasonic bath and rinsed in inert nitrogen gas flow. Table 2 presents the applied current density-charging time combinations as each microstructure shows a unique hydrogen absorption behavior. Charging experiments with 24 h (for the 48 h samples) and 48 h (for 72 h samples) charging time at the respective current density showed already comparable hydrogen concentrations (see Table 3 in Sect. 3 Results). From that

Table 2 Charging current density and time combination

Material	Charging current density (mA/cm^2)/time (h)			
	I	II	III	IV
P92 BM	1.50/48	10.00/48	30.00/48	–
P91 AW-WM	0.25/3	0.63/24	1.50/72	10.00/72
P91 PWHT-WM	1.50/72	10.00/72	20.00/72	40.00/72

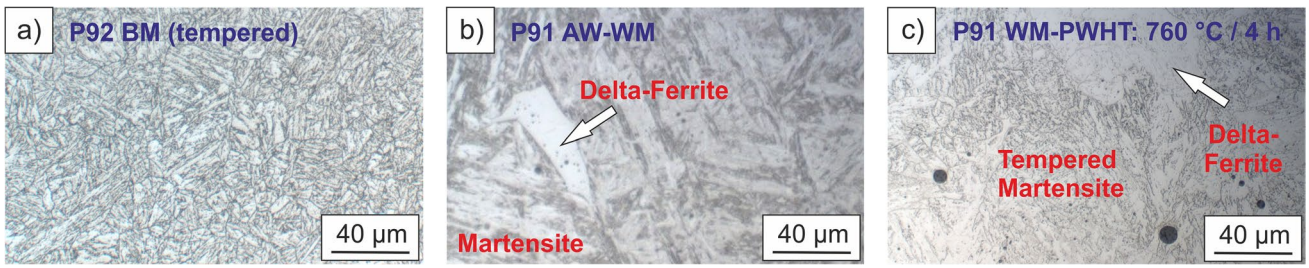

Fig. 2 Microstructure: (a) P92 BM, P91 WM in (b) AW condition, (c) PWHT condition (760 °C for 4 h)

Table 3 Absorbed HD vs. applied charging current density and time combination

Material	Charging current density (mA/cm^2)/time (h)			
	I	II	III	IV
P92 BM	1.50/48	10.00/48	30.00/48	–
HD in ml/100 g	4.1 ± 0.5	6.1 ± 0.5	6.8 ± 0.4	–
P91 AW-WM	0.25/3	0.63/24	1.50/72	10.00/72
HD in ml/100 g	0.8 ± 0.0	1.1 ± 0.2	37.2 ± 6.3	55.3 ± 1.4
P91 PWHT-WM	1.50/72	10.00/72	20.00/72	40.00/72
HD in ml/100 g	3.6 ± 0.4	5.3 ± 0.5	4.6 ± 0.0	7.3 ± 0.2

point of view, a nearly homogenous hydrogen distribution is assumed. Only in case of the charging set I and II for the P91 AW, the short-time charging was necessary to charge only a hydrogen concentration that was comparable to the P92 and the P91 PWHT condition (see Sect. 3 Results). Nonetheless, a certain concentration gradient must always be anticipated in case of electrochemical charging (higher hydrogen activity in electrolyte than in the charged metal/alloy as driving force), e.g., presented in [12, 13, 17, 18, 24, 25].

2.3.2 Hydrogen determination

The diffusible hydrogen concentration "HD" was measured by a G8 Galileo (Bruker AXS, Germany) and a coupled quadrupole mass spectrometer (MS) ESD100 (InProcess Instruments, Germany). This analyzer uses the carrier gas hot extraction (CGHE) technique. In that case, the specimen is heated via infrared radiation-emitting furnace (IR07, part of Galileo G8 system) in a glass tube. The hydrogen in the sample is thermally activated and transported to the MS detection unit via the carrier gas flow (nitrogen 5.0). The ex-ante calibration with different defined amounts of hydrogen volumes allows the precise calibration for the measurement of smallest amounts of hydrogen. Experimental details on the described procedure were presented elsewhere [10, 12, 26]. Before the hydrogen measurement, the sample was defrosted for approximately 40 s in acetone to ambient temperature and subsequently dried in inert nitrogen gas flow for 30 s.

2.3.3 Tensile test

Tensile tests were performed using a Hydropuls PSA with 40 kN maximum test load (Schenk GmbH, Germany) with a crosshead test speed of 1 mm/min. The corresponding test load "F" in kN and the displacement "s" in mm (crosshead of the tensile test machine) were permanently measured and recorded. The ultimate tensile strength (UTS) in MPa was calculated from the maximum test load (in N) and dived by the initial cross section of the sample (approximately 7.065 mm^2, using the initial diameter in the gage section of 3 mm, see Fig. 1c). The local strain in the gage section was not measured by the common (tactile) extensometer. The reasons are as follows: (1) the expected high degree of notch sensitivity (especially in case of the P91 AW-WM), which can influence the fracture position. (2) The additional time for mounting and dismantling of the extensometer influences the detectable hydrogen concentration by CGHE and reduces the reliability of these measurements. For that reason, the corresponding 0.2% offset yield strength (in MPa, if applicable) was approximated from the load–displacement curves in accordance with conventional tensile tests. The maximum elongation at fracture "EL_{max}" in mm was the maximum displacement before the sample ruptured and was used as approximate solution for the ductility (strain was not separately measured).

Before each tensile test, the specimen was defrosted in acetone for approximately 45 s to achieve ambient temperature. Accompanying experiments with different exposition times at ambient temperature showed an average hydrogen loss of 10 to 15% after the stop of hydrogen charging, tensile testing, and the final hydrogen determination. After the tensile test, one-half of the fractured sample was used for the ex-situ assessment of the ductility and fracture topography. For the ductility, the diameter after fracture was measured using a light optical microscopy Polyvar Met (Reichert-Jung, Germany) with an attached Gryphax Altair digital camera (Jenoptik, Germany) and a digital imaging software Imagic (IMS Bildmanagement-System, Switzerland). The diameter of the fractured cross section was estimated from the mean value of at least two digitally measured diameters. The corresponding fracture topography was identified using a desktop scanning electron microscope Phenom XL G2 (Thermo Fisher Scientific, Germany). The other half of the sample was used for the determination of the corresponding HD via CGHE. For that purpose, it was immediately stored in liquid nitrogen at − 196 °C to prevent the hydrogen effusion until the hydrogen measurement. In advance to the test, the remaining screw head was cut off by a bolt cutter, which allowed the determination of the corresponding HD of the gage section only.

3 Results and discussion

3.1 Tensile properties

3.1.1 Hydrogen free references

Figure 3 exemplarily shows load displacement curves for all hydrogen-free reference conditions. It is obvious that the P91 AW-WM significantly differs from the two other conditions due to the increased maximum tensile load "F" of 8.0 kN to 9.2 kN vs. approx. 4.8 kN (P91 PWHT-WM) and 5.1 kN (P92 BM). This approximately corresponds to an UTS from

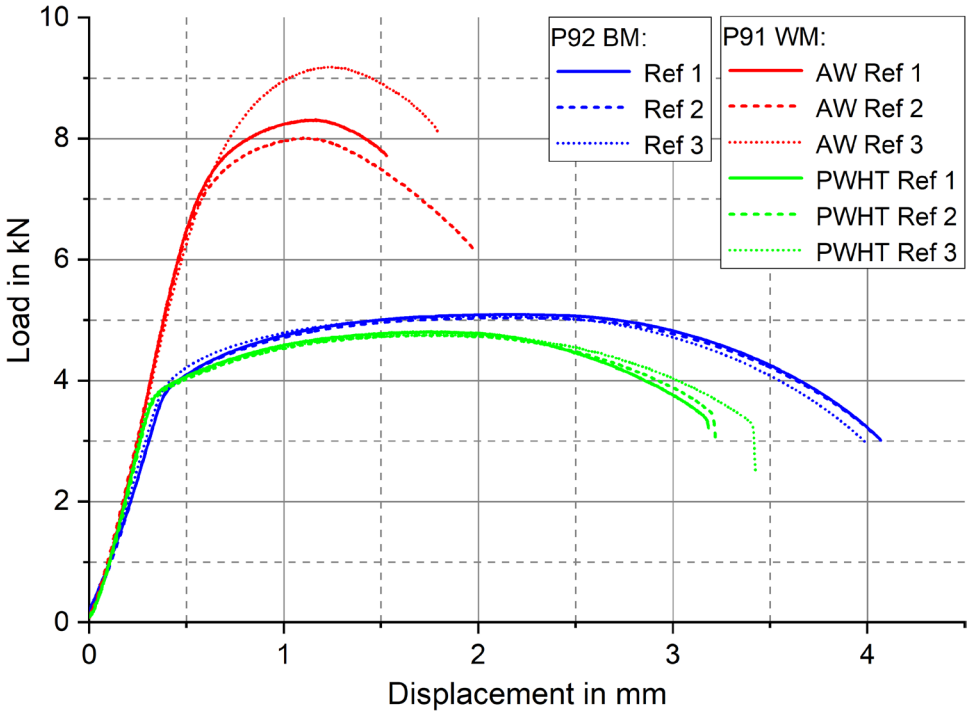

Fig. 3 Load displacement curves for P92 BM, P91 AW-WM, and PWHT-WM

1130 to 1300 MPa compared to averaged 680 MPa (P91 AW-PWHT condition), as well as 720 MPa (the annealed P92 BM). The increase of the UTS in case of the P91 AW-WM is a result of the significant hardening (see Sect. 2.2) compared to the tempered condition in case of the P91 PWHT-WM or the annealed condition of the P92 BM. The most important effect in terms of any HAC susceptibility is the already drastically reduced ductility. The P91 AW-WM ruptured at a maximum elongation/displacement "EL_{max}" of 1.6 to 2.0 mm compared to the 3.2 to 3.4 mm in PWHT condition. In addition, the P92 BM ruptured at a comparable "EL_{max}" of 3.9 to 4.1 mm.

3.1.2 Hydrogen-charged samples

Table 3 summarizes the obtained and measured diffusible HD vs. the applied charging parameter sets (see Table 2). For that reason, the calculated mean values are presented along with their standard deviation. The relative maximum deviation was maximum 10%. All microstructures showed increased absorbed HD with increasing charging current density. The P91 AW-WM had the highest apparent solubility with HD > 50 ml/100 g Fe. The P91 PWHT-WM and the tempered condition of the P92 BM had comparable maximum HDs with 7.3 ml/100 g Fe (P91 PWHT-WM) vs. 6.8 ml/100 g Fe (P92 BM). This means that the heat treatment condition had a significant effect on the hydrogen solubility of the microstructure for a given set of charging current densities. Figure 4 shows the hydrogen influenced load displacement curves for (a) P92 BM, (b) P91 AW-WM and (c) P91 PWHT-WM. Figure 5 shows the summarized "R_m","$R_{p0.2}$" and "EL_{max}" values depending on the respective HD, whereas 0 ml/100 g Fe indicates the uncharged condition (as shown in Fig. 3).

Generally, all investigated microstructures showed a pronounced effect of hydrogen on the mechanical properties, whereas the annealed P92 BM and the tempered P91 PWHT-WM showed comparable behavior within a HD range from 0 ml/100 g Fe to 7 ml/100 g Fe. In both cases, the increasing HD (see Table 3) correlates with a reduction of the achieved displacement (P92 BM: Fig. 4a and PWHT-WM: Fig. 4c), whereas "R_m" (Fig. 5a) and "$R_{p0.2}$" (Fig. 5b) are virtually not affected. The hydrogen effect can be numerically expressed in the achieved maximum elongation at fracture "EL_{max}." As shown in Fig. 5c, the P92 BM (black hatched area) shows a moderate decrease of ductility of approximately up to 4 ml/100 g Fe. Above 6 ml/100 g Fe, a significant loss of the ductility occurs. The P91 PWHT-WM (blue hatched region in Fig. 5c) showed this behavior already above 4 ml/100 g Fe, expressed by the maximum elongation of 0.6 mm compared to approximately 3 mm in the uncharged condition. At the same time, some tensile samples kept a moderate ductility at comparable hydrogen levels. The reason is assumed to be within the heterogeneous microstructure of the P91 multi-layer weld metal, also in PWHT-condition, which corresponds to a nearly fully embrittled material (see Sect. 3.2). It was shown that different charging current densities are necessary to identify a persistent description of the material behavior in the presence of hydrogen. In [24, 25, 27, 28], comparable absorbed HDs of up to 6 ml/100 g were reported for chemically similar but low-alloyed 2.25 Cr and 1.00 Mo (weight %) steels accompanied by a continuous decrease of the ductility. If the P92

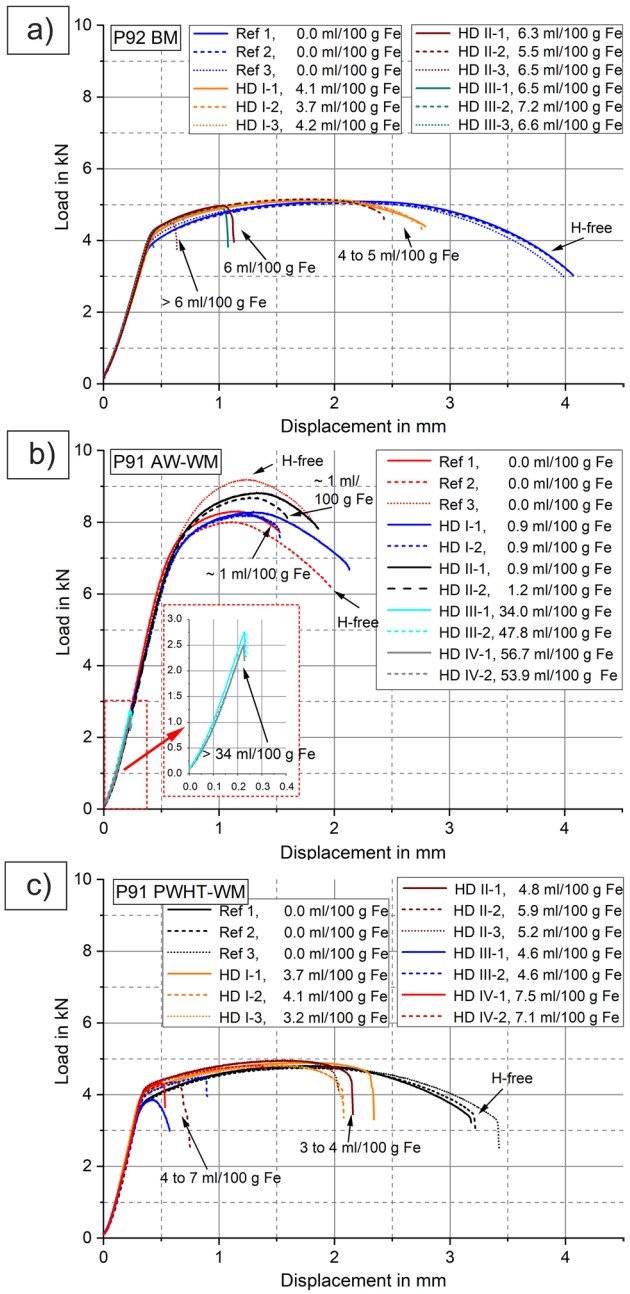

Fig. 4 Load displacements curves for the different HD levels vs. hydrogen free reference: a) P92 BM, b) P91 AW-WM, and c) P91 PWHT-WM

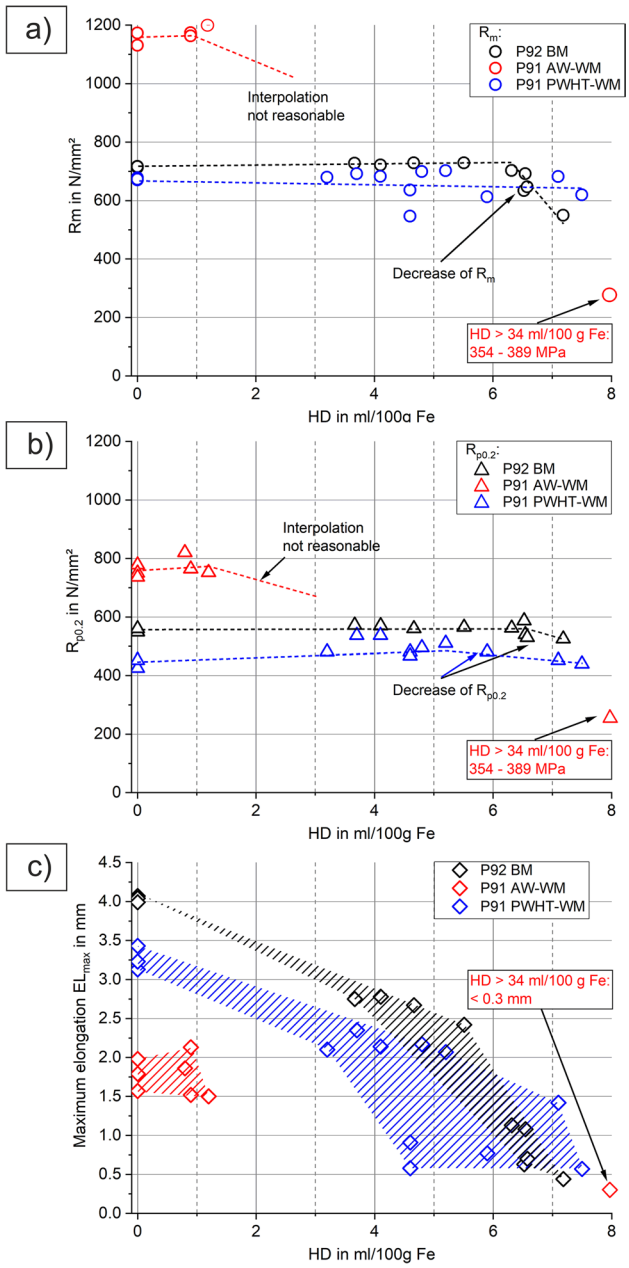

Fig. 5 Summarized mechanical properties for all investigated microstructures: a) Ultimate tensile strength R_m, b) Yield strength $R_{p0.2}$, and c) maximum elongation EL_{max}

BM and P91 WM are compared, the influence of the heat treatment condition is clearly visible in terms of improved ductility especially for the AW-WM. This means that the PWHT (besides its intended use improvement of mechanical properties) is beneficial for the avoidance of HAC due to the tempering of the hardened AW microstructure.

In contrast, the P91 AW-WM showed a two-faced behavior. The charged HD was ≤ 1.2 ml/100 g Fe and ≥ 34 ml/100 g Fe (see Table 3 and Fig. 4b). Different electrochemical charging parameter aiming at lower HDs could not successfully be applied (corroded surfaces, etc.) due to the limited amount of AW-WM tensile samples. In addition, the generally increased hydrogen solubility and trapping efficiency were reported in [24] and in the previous work of the authors [17, 18] of the present study. The higher absorbed concentration is attributed to the as-welded heterogeneous weld metal in terms of the very high number of hydrogen traps, e.g., dislocations that are present in the AW condition annihilate during the PWHT [22, 25]. In addition, the formation and

coarsening of the carbides like $M_{23}C_6$ or MC-like (where "M" means metal, e.g., Cr, Mo, and especially V) [29–33] during PWHT decrease the number of hydrogen traps. Of course, this influenced the mechanical behavior of the tensile samples. As shown in Fig. 3, the ductility of the AW-WM (in hydrogen free condition) is already reduced compared to the P92 BM or P91 WM in PWHT condition. In case of a HD of max. 1.2 ml/100 g Fe, neither the strength nor the ductility was significantly reduced. In case of the high charged HD, the samples ruptured way before reaching "R_m," i.e., even the approximated "$R_{p0.2}$" was not reached. This means the material behavior of the P91 AW-WM was between "not remarkably" influenced to fully embrittled (see fracture topography in Sect. 3.2). As a result, no transient description of the P91 AW-WM behavior was possible, i.e., it was not reasonable to interpolate the behavior between the low and high HD.

Nonetheless, a pronounced effect of hydrogen on the martensitic AW-WM is assumed. In [15], a HD of 1 ml/100 g Fe was reported as HAC critical for a welded joint in conventional cold cracking tests. The authors of the present study cannot directly confirm this result, but the conducted tensile samples of the P91 PWHT-WM suggest that a certain degradation already occurs at HD levels of less than 3 to 4 ml/100 g Fe (if the very moderate material behavior of the PWHT condition is anticipated). Hence, any quenched/as-welded condition must show an increased susceptibility for HAC. It is clearly visible that the degradation intensity varies with both the microstructure and the heat-treatment condition. Generally, the AW condition corresponds to an as-quenched martensite and is the most HAC susceptible microstructure, although a certain short-term annealing would have been estimated due to the multi-layer welding. Considering the reported very low hydrogen diffusion coefficients of the P91 AW-WM compared to the P91 PWHT-WM (in accordance with [17, 18]), a very high risk for time-delayed HAC must be anticipated. This gets especially important for in-service repair welding of components if they are previously exposed to hydrogen containing atmospheres.

3.2 Fractography

The previously described mechanical properties were correlated with the fracture topographies, examined by SEM. For that reason, Fig. 6 shows the P92 BM, Fig. 7 the P91 AW-WM, and Fig. 8 the P91 PWHT-WM. The part (a) shows the uncharged reference with HD = 0 ml/100 g Fe and is continued by respective figures of hydrogen charged samples with different HDs in parts (b) to (d). Some sets of the applied charging parameters were assumed to result in a heterogeneous hydrogen distribution, e.g., due to short charging time like in case of the P91 AW-WM (see Table 2). The CGHE only allows to determine an overall hydrogen concentration in the sample. For that reason, different regions of the fracture surfaces were examined assuming different hydrogen diffusion depths. In Fig. 6 to Fig. 8, the sub-part "I." shows the fracture topography in the center and sub-part "II." in the surface near region. The abbreviations for the fracture topography characteristics are "D" - ductile, "QC" - quasi-cleavage, "C" - cleavage, and "IG" - intergranular fracture.

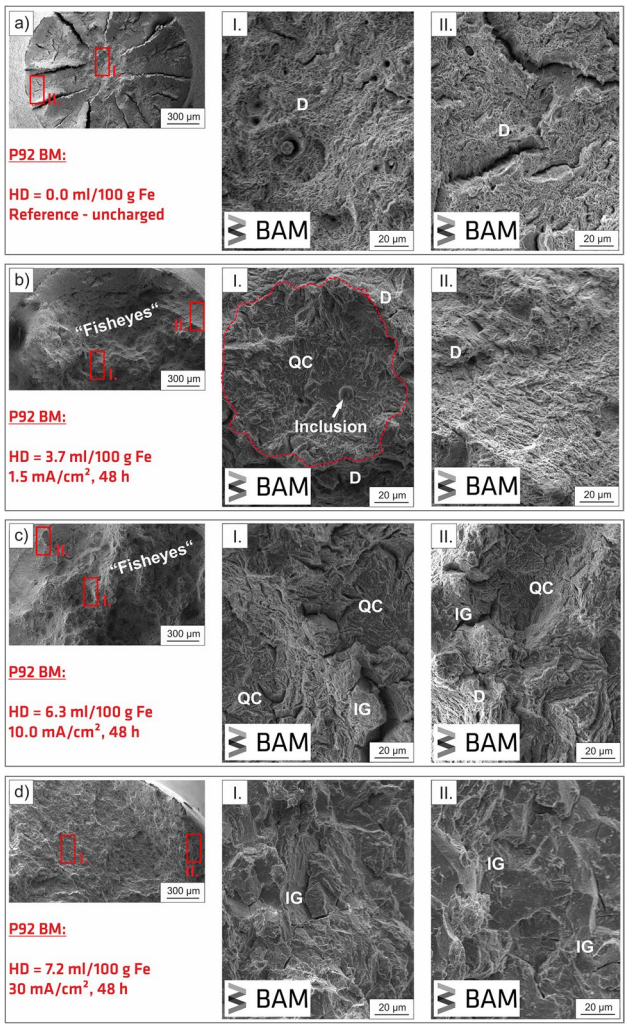

Fig. 6 P92 BM fracture topography: (a) uncharged reference HD = 0 ml/100 g Fe, (b) HD = 3.7 ml/100 g Fe, (c) HD = 6.3 ml/100 g Fe, and (d) 7.2 ml/100 g Fe, I. showing center and II. surface near position

The uncharged samples show the typical ductile behavior, which is indicated by the pronounced dimpled (D) topography (see Fig. 6a to Fig. 8a). The hydrogen effect on the mechanical properties is clearly visible in terms of changing fracture topographies as shown in the corresponding parts (b to d). Depending on the material hardness, i.e., ductility, hydrogen causes "fisheyes" in the P92 BM at HD = 3.7 ml/100 g. These fisheyes represent locally embrittled areas around material defects like inclusions and are characterized by quasi-cleavage (QC) facets within a ductile (dimpled) topography [34, 35]. The reason is that during straining of the sample, mechanical

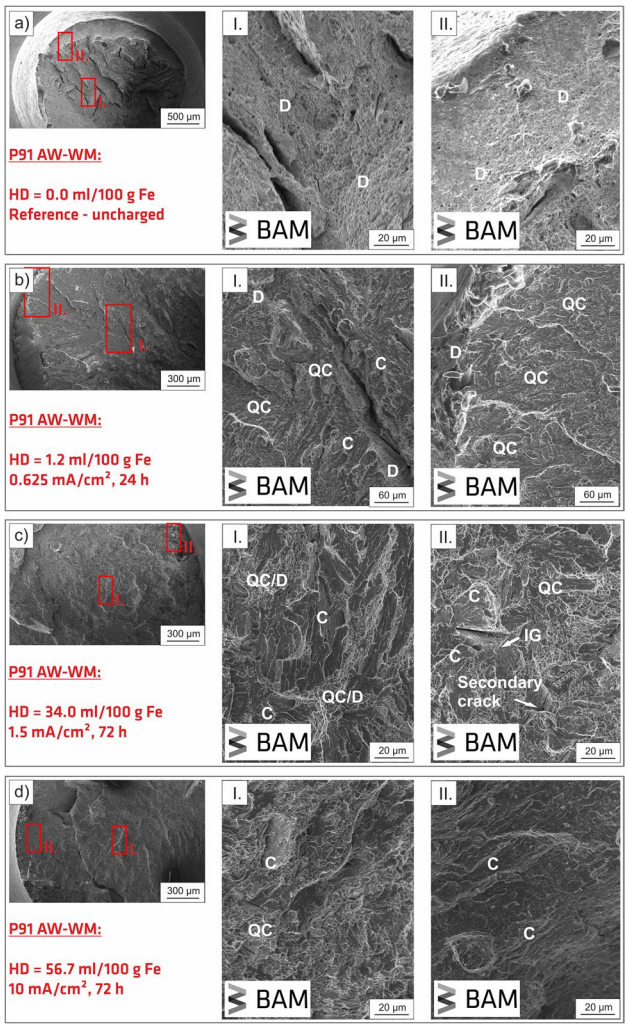

Fig. 7 P91 AM-WM fracture topography: (a) uncharged reference HD = 0 ml/100 g Fe, (b) HD = 1.2 ml/100 g Fe, (c) HD = 34.0 ml/100 g Fe, and (d) 56.7 ml/100 g Fe, I. showing center and II. surface near position

stresses concentrate around the inclusion and the more or less evenly distributed dissolved hydrogen preferably diffuses into these regions and accumulates. The higher HD (in that case) embrittles very local areas. These are typical HAC features during tensile tests. The appearance just in surface near regions in the tensile sample (Fig. 7b, sub-part II) suggests that the chosen charging parameters were perhaps insufficient for the desired diffusion depth and the charging time would have to be increased. Nonetheless, if the HD is further increased to 6.3 ml/100 g Fe (Fig. 7c) and 7.2 ml/100 g Fe (Fig. 7d), the fracture topography changes to QC and finally to intergranular (IG) fracture and explains the sudden decrease of the mechanical strength at this HD level (Fig. 5a). This significant change within a small deviation of the entire HD range emphasizes the necessity of transient fracture criteria with different HD levels [12, 13, 24, 27].

The P91 WM showed in both conditions a distinct change of the fracture topography dependent on the respective HD. In the AW condition already a HD of 1.2 ml/100 g Fe results in a distinct embrittlement (QC facets in the center and surface near region as shown in Fig. 7b). The highest absorbed concentrations (shown in Figs. 7c, d) resulted in merely pure QC or C fracture topography, which supports the identified significant decrease of the tensile strength (Fig. 5a) and virtually no ductility (Fig. 5c). In contrast, the PWHT resulted in comparable fracture topographies to the P92 BM. At HD of 3.7 ml/100 g Fe (Fig. 8b) and 5.9 ml/100 g Fe (Fig. 8c), a mixture of dimpled structures and the already mentioned "fisheyes" with QC surrounded by ductile topography can be found. Increasing HD to 7.5 ml/100 g Fe (Fig. 8d) resulted in a cleavage (C) topography in the center (sub-part I.) and surface near area (sub-part II.) indicating the total embrittlement.

The obtained results allow the description of the hydrogen effect on a microscopic scale for the different charged HD levels with ductile fracture (D), indicating a high deformation during the tensile test, mostly appearing at $0 < HD < 4$ ml/100 g Fe, quasi-cleavage fracture (QC), with moderate deformation ability, appearing at $1 < HD < 6$ ml/100 g Fe, cleavage fracture (C), appearing at $HD > 7$ ml/100 g Fe, and intergranular fracture (IG), appearing $HD > 6$ ml/100 g Fe. Typically, C and IG fracture topographies are distinct identifiers for the strong embrittlement due to the presence of hydrogen. This is in accordance with the presented mechanical data in Sect. 3.1.

3.3 Fracture criteria

Due to the complex interaction of HD and the microstructure, the changing mechanical properties must be assessed. For that reason, the true strain "ε_T" was applied in the present study. The true strain concept is defined in Eq. 1, where "A_0" is the initial cross section and "A_f" the cross section after fracture [36].

$$\varepsilon_T = \ln\left(\frac{A_0}{A_f}\right) \tag{1}$$

The degradation was then expressed by a regression analysis using a parametrized exponential decay function (fit routine in ORIGIN 9.6) per microstructure. Figure 9 shows the obtained regression curves and the achieved model quality (least square sum, "R^2"). Equation 2 shows the used regression function and Table 4 shows the corresponding parameters, whereas "A" is a material specific constant, "B" is the pre-exponential factor, "K" is a HD constant (in ml/100 g Fe), and "L" a correction parameter for the entire slope of the regression function (in ml/100 g Fe).

$$\varepsilon_T = A + B * e^{\left[-\frac{(HD-K)}{L}\right]} \tag{2}$$

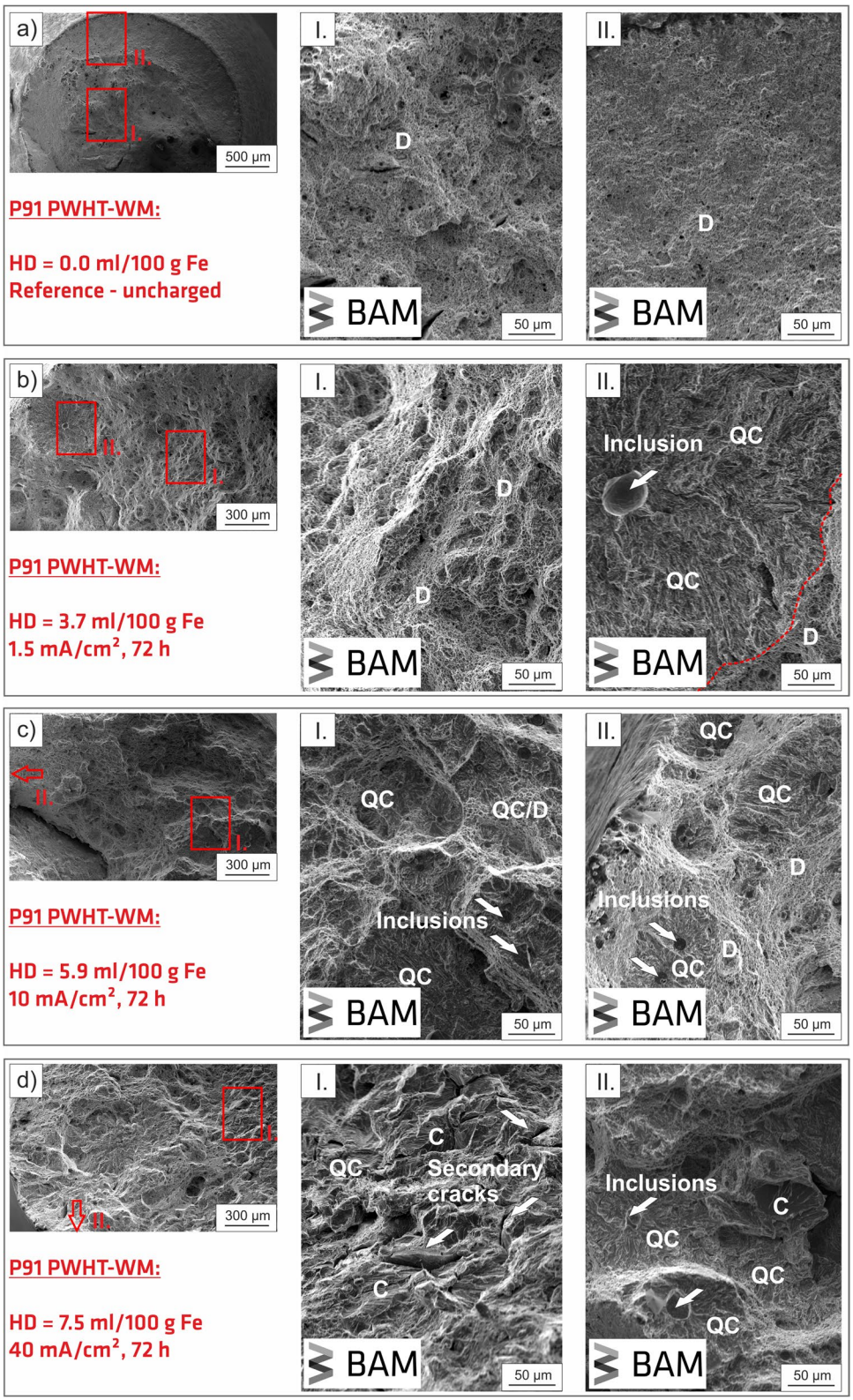

Fig. 8 P91 PWHT-WM fracture topography: (a) uncharged reference HD = 0 ml/100 g Fe, (b) HD = 3.7 ml/100 g Fe, (c) HD = 5.9 ml/100 g Fe, and (d) 7.5 ml/100 g Fe

Compared to the tensile values (Figs. 5a, b), the influence of hydrogen on the material ductility can be described by mathematical regression functions using the true elongation concept. This procedure allows a *microstructure-specific and quantitative* assessment of the HAC susceptibility of a welded joint [12, 13, 37], and especially for high-alloyed [38] or creep-resistant

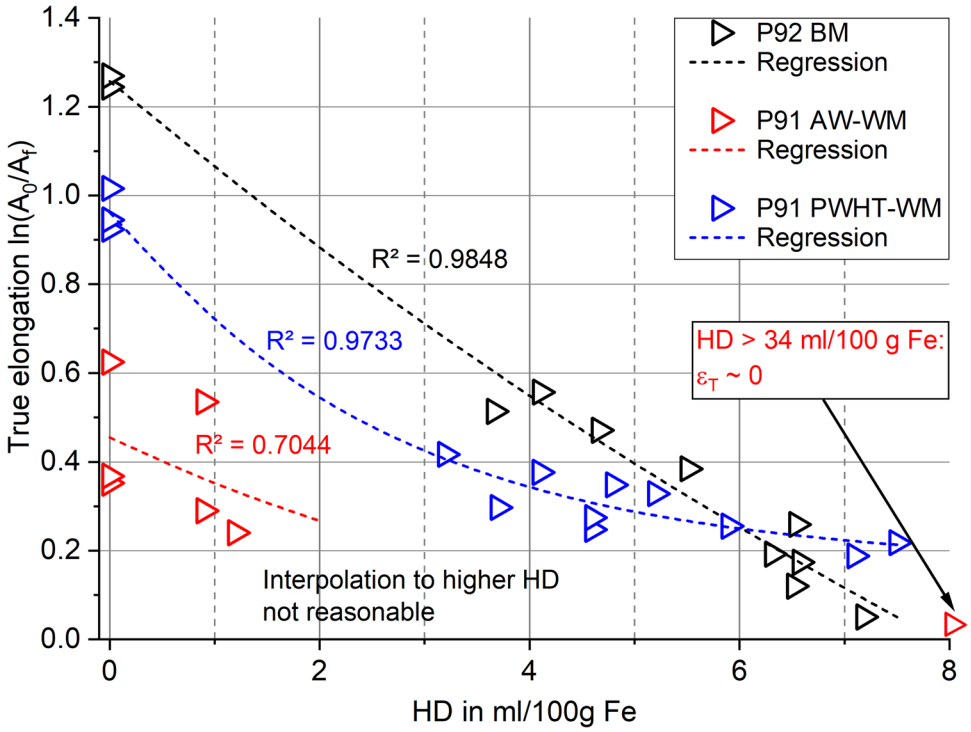

Fig. 9 Regression functions for the true strain vs. the hydrogen concentration

Table 4 Regression functions for the different microstructures and corresponding HD ranges

Microstructure	*A*	*B*	*K*	*L*	HD range in ml/100 g
P92 BM	−2.115	2.205	7.193	16.930	0.0 to 7.2
P91 AW-WM	0.018	0.365	0.730	3.551	0.0 to 1.1 (56.7)
P92 PWHT-WM	0.169	0.751	0.140	2.596	0.0 to 7.5

CrMo steels [28]. Envelope curves can describe the region, in which a certain ductility allows a corresponding "safe" HD, whereas a lower curve would represent the conservative engineering approach for HAC as all data points below this curve mean "no crack." Due to the low scattering of the present data, no envelope curves were defined as HAC criteria. The suggested regression would perhaps have to be corrected by a safety factor. Nonetheless, a big advantage of the suggested concept is the persistent description of the hydrogen-dependent degradation behavior that allows advantages compared to further analytical concepts. The embrittlement index "EI" [27, 28, 39] only allows a qualitative ranking between 0 % (fully ductile) and 100 % (fully embrittled). In contrast, the true elongation concept can be used for numerical simulation of HAC in steel weld joints. It directly allows the numerical calculation of HAC for each different weld joint microstructure and the specific assessment of the crack appearance based on a known hydrogen ingress or the maximum tolerable hydrogen concentration for safe welding fabrication [40–42].

4 Conclusions

The focus of this study was the microstructure and heat treatment effect on the mechanical properties of P92 base material and P91 multi-layer weld metal. Tensile tests with hydrogen-free reference samples and hydrogen-charged samples were carried out, the mechanical properties were assessed and supported by dedicated fractographic analysis. In addition, hydrogen and microstructure-dependent fracture criteria were calculated. The following conclusions can be drawn:

- In hydrogen-free condition, the martensitic P91 AW-WM showed a significantly increased tensile strength and reduced ductility as a result of the increase of the hardness to 404HV0.5. The hardness of the tempered P91 PWHT-WM was comparable to the normalized and tempered P92 BM. All microstructures showed a hydrogen influenced degradation of the mechanical properties with a strong relation to the absorbed hydrogen concentration. In that connection, the P91 AW-WM had the highest degree of degradation in the presence of hydrogen but was accompanied by the highest absorbed concentration levels of more than 50 ml/100 g Fe.
- The degradation of the mechanical properties was clearly identified for each microstructure by distinct SEM investigations. In hydrogen-free condition, dimpled topographies were found indicating the ductile predominant frac-

ture of the sample. In hydrogen-charged condition, the dimpled areas are more and more replaced by embrittled regions. Fisheyes, quasi-cleavage facets, intergranular, and secondary cracks can be found in this order with increasing absorbed hydrogen concentrations.

- The application of the true strain concept allows the persistent description of the hydrogen-influenced and microstructure-specific degradation. In that connection, hydrogen concentration-based and microstructure-specific persistent fracture criteria were proposed and shown for the first time for P92 BM and P91 WM in both conditions.
- Based on the presented results, it must be anticipated that any hardened P91/P92 weld microstructure must be regarded as highly susceptible for HAC and requires careful welding fabrication. That means a HRHT/DHT is mandatory after welding if the welding sequence is interrupted or the PWHT is delayed.

Acknowledgements Marina Marten and Mareike Kirstein are thanked for their assistance with metallographic preparation; Kjell Erxleben is recognized for his valuable assistance during the microscopic investigations, all with Bundesanstalt für Materialforschung und -prüfung (BAM), Berlin. In addition, Dr.-Ing. Lei Zhang (formerly BAM, now with Tesla Manufacturing GmbH, Gruenheide (Mark), Germany) is thanked for her fruitful comments.

Funding Open Access funding enabled and organized by Projekt DEAL. Open Access funding enabled and organized by Projekt DEAL.

Data availability The raw data is not accessible by the public but can be shared on demand with private access.

Declarations

Competing interests The authors declare no competing interests.

References

1. Hahn B, Bendick W (2008) Rohrstähle für moderne hochleistungskraftwerke. 3R International 47:3–12
2. Coleman KK, Newell WF Jr (2007) P91 and beyond - welding the new-generation Cr-Mo alloys for high-temperature service. Weld J 86(8):29–33
3. Aguero A, Audigie P, Rodriguez S et al. Protective coatings for high temperature molten salt heat storage systems in solar concentration power plants. SolarPACES2017 Conference, AIP Conference Proceedings 2033(1):90001–1–090001–8; 2017. https://doi.org/10.1063/1.5067095
4. Mukherjee S, Jamnapara NI (2015) Materials research and development opportunities in fusion reactors. Proc Indian Natn Sci Acad 81(4):827–839. https://doi.org/10.16943/ptinsa/2015/v81i4/48299
5. Brozda J (2005) New generation creep-resistant steels, their weldability, and properties of welded joints: T/P92 steel. Weld Int 19(1):5–13. https://doi.org/10.1533/wint.2005.3370
6. Lojen G, Vuherer T (2020) Optimization of PWHT of simulated HAZ subzones in P91 steel with respect to hardness and impact toughness. Metals 10(9):1215. https://doi.org/10.3390/met10091215
7. Husemann RU, Devrient S, Kilian R (2012) Cracking mechanism in high temperature water-T24 root cause analysis program. In: Proceedings of the 38th VDI-Jahrestagung Schadensanalyse in Kraftwerken. VDI-Wissensforum, Düsseldorf, pp 87–103
8. Garet M, Brass AM, Haut C et al (1998) Hydrogen trapping on non-metallic inclusions in Cr-Mo low alloyed steels. Corros Sci 40:1073–1086. https://doi.org/10.1016/S0010-938x(98)00008-0
9. Albert SK, Ramasubbu V, Parvathavarthini N et al (2003) Influence of alloying on hydrogen-assisted cracking and diffusible hydrogen content in Cr-Mo steel welds. Sadhana 28:383–393. https://doi.org/10.1007/bf02706439
10. Steppan E, Mantzke P, Steffens BR et al (2017) Thermal desorption analysis for hydrogen trapping in microalloyed high-strength steels. Weld World 61:637–648. https://doi.org/10.1007/s40194-017-0451-z
11. ISO 17642-1:2004 Destructive tests on welds in metallic materials - cold cracking tests for weldments - arc welding processes - part 1: general; German version EN ISO 17642-1:2004. Beuth-Verlag, Berlin, Germany. https://doi.org/10.31030/9519379
12. Rhode M (2016) Hydrogen diffusion and effect on degradation in welded microstructures of creep-resistant low-alloyed steels. BAM-Dissertationsreihe No. 148, Bundesanstalt für Materialforschung und -prüfung (BAM), Berlin, Germany
13. Rhode M, Steger J, Steppan E et al (2016) Effect of hydrogen on mechanical properties of a reactor pressure vessel steel grade. Weld World 60(4):623–638. https://doi.org/10.1007/s40194-016-0325-9
14. Pillot S, Coudreuse L (2012) Hydrogen induced disbonding and embrittlement of steels used in petrochemical refining. In: Gangloff RP, Somerday BP (eds.) Gaseous Hydrogen embrittlement of Materials in Energy Technologies, Vol. 1: The problem, its characterization and effects on particular alloy classes. Woodhead Publishing, Cambridge, United Kingdom 51–93. https://doi.org/10.1533/9780857093899.1.51
15. Chakraborty G, Rejeesh R, Venkata Ramana O et al (2020) Evaluation of hydrogen-assisted cracking susceptibility in modified 9cr-1mo steel welds. Weld World 64:115–122. https://doi.org/10.1007/s40194-019-00812-2
16. EN ISO 3690:2018 Welding and allied processes - determination of hydrogen content in arc weld metal (ISO 3690:2018); German version EN ISO 3690:2018. Beuth-Verlag, Berlin, Germany. https://doi.org/10.31030/3002668
17. Rhode M, Richter T, Mente M et al (2022) Thickness and microstructure effect on hydrogen diffusion in creep-resistant 9% Cr P92 steel and P91 weld metal. Weld World 66:325–340. https://doi.org/10.1007/s40194-021-01218-9
18. Rhode M, Richter T, Mente M et al (2020) Hydrogen diffusion in creep-resistant 9% Cr P91 multi-layer weld metal. Weld World 64:267–281. https://doi.org/10.1007/s40194-019-00828-8
19. Manufacturer specification for welding wire Böhler C 9 MV Ti-FD. voestalpine Böhler Welding Group GmbH, Hamm,

Germany, 2015. via: https://www.kskct.cz/images/katalog/dratyna-civkach-trubickove/dokumentace/L1_3455_en__B_Boehler%20c%209%20mv%20ti-fd_fde_en_5%20(1).pdf
20. EN 10216–2:2014 Seamless steel tubes for pressure purposes - technical delivery conditions - part 2: non-alloy and alloy steel tubes with specified elevated temperature properties; German version EN 10216-2:2013. Beuth-Verlag, Berlin, Germany. https://doi.org/10.31030/3068303
21. EN ISO 17634:2015 Welding consumables - tubular cored electrodes for gas shielded metal arc welding of creep-resisting steels - classification (ISO 17634:2015); German version EN ISO 17634:2015. Beuth-Verlag, Berlin, Germany. https://doi.org/10.31030/2353520
22. Pandey C, Mahapatra MH, Kumar P et al (2018) Some studies on P91 steel and their weldments. J Alloys Compd 743:332–364. https://doi.org/10.1016/j.jallcom.2018.01.120
23. Salmi S, Rhode M, Juettner S et al (2014) Hydrogen determination in 22MnB5 steel grade by use of carrier gas hot extraction technique. Weld World 59:137–144. https://doi.org/10.1007/s40194-014-0186-z
24. Dayal RK, Parvathavarthini N (2003) Hydrogen embrittlement in power plant steels. Sadhana 28:431–451. https://doi.org/10.1007/bf02706442
25. Parvathavarthini N, Saroja S, Dayal RK (1999) Influence of microstructure on the hydrogen permeability of 9%Cr-1%Mo ferritic steel. J Nucl Mater 264:35–47. https://doi.org/10.1016/S0022-3115(98)00486-3
26. Rhode M, Schaupp T, Muenster C et al (2018) Hydrogen determination in welded specimens by carrier gas hot extraction-a review on the main parameters and their effects on hydrogen measurement. Weld World 63:511–526. https://doi.org/10.1007/s40194-018-0664-9
27 Xu H, Xia X, Hua L et al (2012) Evaluation of hydrogen embrittlement susceptibility of temper embrittled 2.25Cr-1Mo steel by SSRT method. Eng Fail Anal 19:43–50. https://doi.org/10.1016/j.engfailanal.2011.08.008
28. Rhode M, Steger J, Boellinghaus T et al (2016) Hydrogen degradation effects on mechanical properties in T24 weld microstructures. Weld World 60:201–216. https://doi.org/10.1007/s40194-015-0285-5
29. Fallahmohammadi E, Bolzoni F, Fumagalli G et al (2014) Hydrogen diffusion into three metallurgical microstructures of a C-Mn X65 and low alloy F22 sour service steel pipelines. Int J Hydro Energ 39(25):13300–13313. https://doi.org/10.1016/j.ijhydene.2014.06.122
30. Pandey C, Mahapatra MM (2016) Effect of heat treatment on microstructure and hot impact toughness of various zones of P91 welded pipes. J Mater Eng Perform 25:2195–2210. https://doi.org/10.1007/s11665-016-2064-x
31. El-Rahman MA, El-Salam A, El-Mahallawi I et al (2013) Influence of heat input and post-weld heat treatment on boiler steel P91 (9Cr-1Mo-V-Nb) weld joints. J Heat Treat Surf Eng 7(1):32–37. https://doi.org/10.1179/1749514813Z.00000000051
32. Hurtado-Norena C, Bruzzoni P (2010) Effect of microstructure on hydrogen diffusion and trapping in a modified 9%Cr-1%Mo steel. Mater Sci Eng A 527(3):410–416. https://doi.org/10.1016/j.msea.2009.08.025
33. Saini N, Mulik RS, Mahapatra MM (2019) Influence of filler metals and PWHT regime on the microstructure and mechanical property relationships of CSEF steels dissimilar welded joints. Int J Pres Ves Pip 170:1–9. https://doi.org/10.1016/j.ijpvp.2019.01.005
34. Lynch SP (2012) Hydrogen embrittlement phenomena and mechanisms. Corr Rev 30:105–123. https://doi.org/10.1515/corrrev-2012-0502
35. Martin ML, Fenske JA, Liu GS et al (2011) On the formation and nature of quasi-cleavage fracture surfaces in hydrogen embrittled steels. Acta Mater 59(4):1601–1606. https://doi.org/10.1016/j.actamat.2010.11.024
36. Davies JR (2004) Tensile testing, 2nd edn. ASM-International, Materials Park
37. Zimmer P (2007) Zur bewertung der kaltrisssicherheit von schweißverbindungen aus hochfesten feinkornbaustählen. BAM-Dissertationsreihe No. 29, Bundesanstalt für Materialforschung und -prüfung (BAM), Berlin, Germany
38. Boellinghaus T, Hoffmeister H (2000) Numerical model for hydrogen assisted cracking. Corrosion 56(6):611–622. https://doi.org/10.5006/1.3280564
39. Depover T, Perez Escobar D, Wallaert E et al (2014) Effect of hydrogen charging on the mechanical properties of advanced high strength steels. Int J Hydrog Energ 39:4647–4656. https://doi.org/10.1016/j.ijhydene.2013.12.190
40. Mente T (2014) Numerische Simulation der wasserstoffunterstützten Rissbildung in austenitisch-ferritischen Duplexstählen. BAM-Dissertationsreihe No. 129, Bundesanstalt für Materialforschung und -prüfung (BAM), Berlin, Germany
41. Wongpanya P, Boellinghaus T, Lothongkum G et al (2009) Numerical modeling of cold cracking initiation and propagation in S 1100 QL steel root welds. Weld World 53:R34–R43. https://doi.org/10.1007/bf03266701
42. Mente T, Boellinghaus T, Schmitz-Niederau M (2012) Heat treatment effects on the reduction of hydrogen in multi-layer high-strength welds. Weld World 56:26–36. https://doi.org/10.1007/bf03321362